BMC Medical Imaging

RESEARCH

Open Access

Knowledge discovery from database: MRI radiomic features to assess recurrence risk in high-grade meningiomas

Chen Chen[1*†], Lifang Hao[2†], Bin Bai[3†] and Guijun Zhang[4]

Abstract

Purpose We used knowledge discovery from radiomics of T2-weighted imaging (T2WI) and contrast-enhanced T1-weighted imaging (T1C) for assessing relapse risk in patients with high-grade meningiomas (HGMs).

Methods 279 features were extracted from each ROI including 9 histogram features, 220 Gy-level co-occurrence matrix features, 20 Gy-level run-length matrix features, 5 auto-regressive model features, 20 wavelets transform features and 5 absolute gradient statistics features. The datasets were randomly divided into two groups, the training set (~ 70%) and the test set (~ 30%). Combinations of data preprocessing methods, including normalization (Min-Max, Z-score, Mean), dimensionality reduction (Pearson Correlation Coefficients (PCC)), feature selector (max-Number, cluster) and ten-fold cross-validation were analyzed for their prediction performance. Kaplan–Meier curve, Cox proportional hazards regression model were used and concordance index (C-index), integrated Brier score (IBS) were selected. Model performance was assessed using the C-index.

Results WHO grade, age, gender, histogram (Mean, Perc.90%, Perc.99%), Gray-level co-occurrence matrix (S(3, -3) DifVarnc, S(5, 5)Correlat, S(1, 0)SumEntrp, S(2, -2)InvDfMom), Teta1, WavEnLL_s-2 and GrVariance were identified as the significant recurrence factors. The pipeline using Mean_PCC_Cluster_10 of T1C yielded the highest efficiency with an IBS of 0.170, 0.188, 0.208 and C-index of 0.709, 0.705, 0.602 in the train, test and validation sets, respectively. The pipeline using MinMax_PCC_Cluster_19 of T2WI yielded the highest efficiency with an IBS of 0.189, 0.175, 0.185 and C-index of 0.783, 0.66, 0.649 in the train, test and validation sets. The pipeline using MinMax_PCC_Cluster_13 of T2WI + T1C yielded the highest efficiency with an IBS of 0.152, 0.164, 0.191 and C-index of 0.701, 0.656, 0.593 in the train, test and validation sets, respectively.

Conclusion Knowledge discovery from MRI radiomic features can slightly help predict recurrence risk in HGMs. T2WI or T1C yielded better efficiency than T2WI + T1C. The parameters with the best power were Mean, Perc.99%, WavEnLL_s-2, Teta1 and GrVariance.

Keywords Recurrence, Radiomics, Knowledge discovery, Neoplasms

[†]Chen Chen, Lifang Hao and Bin Bai contributed equally to this work.

*Correspondence:
Chen Chen
934717369@qq.com
Full list of author information is available at the end of the article

Introduction

Meningiomas are the most common intracranial tumor originating from the arachnoid cap cells, which account for 39% of central nervous system neoplasms [1]. Around 5% of all newly diagnosed meningiomas are high-grade meningiomas (HGMs, WHO grade II and III) [2], accompanied with aggressive clinical features and frequent tumor recurrence compared to their benign low-grade meningiomas (LGMs, WHO grade I). The 5-year recurrence rate after total resection of grade I, II, III meningiomas are 7–23%, 50–55%, and 72–78% [3, 4]. Because of the huge difference between LGMs and HGMs, a preoperative model for assessing relapse risk in patients with HGMs should be constructed to help individualized treatment and improve the long-term survival rate.

Conventional magnetic resonance imaging (MRI) has limitations of its own when assessing recurrence risk in HGMs. It is possible to analyze pixel distributions, intensities and dependencies by mathematically defining features in radiomics, and it can provide information that is not visible with the naked eye [5]. Radiomics endeavors to uncover and quantify the concealed information embedded in biomedical images through the application of machine learning (ML) or deep learning methodologies. Analyzing and understanding such vast quantities of data can be effectively accomplished through Knowledge Discovery from Databases (KDD), which stands as an interdisciplinary field encompassing artificial intelligence, databases, statistics, and ML. ML is a branch of artificial intelligence that allows computers to learn from large complex datasets and perform tasks such as analysis, classification and prediction, which has potential to play a key role across a variety of medical imaging applications [6, 7]. To our knowledge, in some studies, they proposed a combination of radiomic analysis and ML or deep learning for classification MRI of most common brain tumours or LGMs and HGMs, predicting mitosis cycles in intracranial meningioma, assessing preoperative risk of subtotal resection in skull meningiomas, predicting of Ki-67 proliferation index or sinus invasion in meningiomas or recurrence in parasagittal and parafalcine meningiomas (WHO grade I) [8–17]. Ko et al. [18] reported MRI radiomics based on support vector machine to predict progression/recurrence in WHO grade I meningiomas and Kalasauskas et al. [19] reported value of radiomic and semantic MRI characteristics for the prediction of WHO grade II meningiomas relapse. Few articles have been reported on the use of radiomics to assess the relapse risk in patients with HGMs. To bridge this gap, this retrospective study was designed to assess the potential value of the KDD-based MRI radiomics for recurrence risk in HGMs.

Materials and methods

Patients

The surgical pathology database at our hospital was utilized from November 1, 2021, to November 1, 2023. Exclusion criteria were (1) patients treated before surgery, and (2) inadequate image quality. All methods were performed according to relevant guidelines. The study was approved by the Institutional Ethics Review Committee of Henan Provincial People's Hospital and all the patients signed informed consent.

Image acquisition

Patients were examined using a 3.0T MRI scanner (Siemens Skyra) with the standard head coil. MRI scan protocols included the following: axial T2WI (TR = 5000 ms, TE = 117 ms, matrix = 256 × 256, intersection gap = 1 mm, thickness = 5 mm and field of view = 24 × 24 cm). Contrast-enhanced T1WI (T1C)(TR = 260.0 ms, TE = 2.46 ms, flow rate = 2.0 mL/s, dose = 0.2 ml/kg).

Textural feature extractions

Analyses were performed using MaZda v. 4.7 software (Institute of Electronics, Lodz Technical University, https://qmazda.p.lodz.pl/) [20–23]. In order to get reliable results on MRI texture classifications, the dynamics were limited to $\mu \pm 3\delta$(μ: mean gray-level value, δ: standard deviation) [24]. The next step was to draw regions of interest (ROIs) on images of T2WI and T1C of the largest lay on 2D sequences. It took two doctors with more than ten years of experience to delineate the ROIs manually along the edges of the lesion, fill the lesion with red markers, and exclude necrotic and cystic tissue intending for the analysis of viable lesions, and the third senior radiologist made the final decision in case of any disputes. In the subsequent analyses, the averages of the measurements were used. The degree of agreement was categorized as follows: an interclass correlation coefficient (ICC) value below 0.60 signified poor to moderate concordance; an ICC ranging from 0.61 to 0.80 indicated good agreement; whereas, an ICC spanning from 0.81 to 1.00 represented excellent agreement. A total of 279 feature values and corresponding histograms were extracted for each ROI. Based on feature classes, the number of radiomics features included (i) 9 histogram features on the basis of the pixel counts in images with specific gray-level values [25], (ii) 220 Gy-level co-occurrence matrix (GLCM) features in accordance with a statistical description of the pixel pair distribution [26], (iii) 20 Gy-level run-length matrix (GLRLM) features, achieved by searching the image for runs with the same gray-level value in predefined directions [27], (iv) 5 auto-regressive model (ARM) features, grounded in the weights attributed to

four adjacent pixels and the variance derived from minimizing the prediction error, (v) 20 wavelets transform (WAV) features, rooted in the extraction of texture frequency components from the energy levels calculated within distinct channels [28] and (vi) 5 absolute gradient statistics (AGS) features, computed according to the analysis of the spatial variation of grey-level values across the entire image [25]. Multiple GLCMs were computed at various distances of 1, 2, 3, and 4 pixels, in the directions of 0°, 45°, 90° and 135° (with respect to the horizontal axis), as well as potentially along the z-axis for volumetric or multi-slice images. Multiple GLRLMs were computed at four distinct angles: horizontal (0°), vertical (90°), diagonal 45, and diagonal 135. Clinical information included age, gender, WHO meningioma grading (grades II and III), relapse time, and the tumor area. Multiple meningiomas from the same patient were considered as a single case in ROI classification and impact feature extraction.

Feature selections

A computer-generated random dataset was used to allocate 70% of the dataset to the training set and the remaining (30%) of the dataset to the independent test set. FeAture Explorer software (FAE; V 0.5.5, https://github.com/salan668/FAE.) was developed using the Python programming language (https://python.org) and NumPy, pandas, and scikit-learning modules (https://scikit-learn.org). The survival analysis module of FAE software was modeled based on Lifelines and PyCox. Firstly, we normalized the dataset by MinMax Normalization, Z-score Normalization and Mean Normalization. Min-max normalization maps the original data range into a new range[0,1] in a linear fashion. Z-score Normalization subtracts the mean value and divides the standard deviation for each feature. Mean Normalization involves calculating the mean (average) value for each feature in a dataset and then subtracting that mean from each feature's value to normalize the data, typically scaling it to a range such as [-0.5, 0.5]. Secondly, we used a Pearson Correlation Coefficient (PCC) to dimension reduction. PCC is used for each pair of features to reduce the row space dimensions of the feature matrix and the PCC is used to reflect the degree of linear correlation between two variables. Its value ranges from −1 to 1, with a larger absolute value indicating a stronger correlation. A PCC value of 0.99, which is often adopted as a criterion in literature, indicates an extremely high degree of linear correlation between the two variables, and this correlation is statistically significant. But if the PCC is greater than 0.99, one of them is randomly deleted in order to reduce data redundancy and enhance model efficiency. Iterate through all features and calculate the Pearson correlation coefficient between each pair. Lastly, we set feature number range from 1 to 20, feature selection through clustering, and ten-fold cross-validation. When selecting the minimum and maximum number of features, FeAture Explorer software will iterate through all possible feature counts within this range to build models. From the perspective of data interpretability, it is advisable to keep the maximum number of features in the model relatively low (e.g., 20). If the number of features being iterated over exceeds the total number of features in the feature matrix, all features will be used for modeling. Cluster specifies what column has unique identifiers for clustering covariances. Using this forces the sandwich estimator (robust variance estimator) to be used. This module splits the training data into a training set and a validation set to find the optimal combination of the aforementioned strategies. In order to seek a stable combination of hyperparameters, a ten-fold cross-validation approach is chosen. Initially, the sampling is divided into 10 subsets, with each subset being held out in turn as the validation data for the model, while the remaining 9 subsets are used for training. This cross-validation process is repeated 10 times, with each subset serving as the validation data once. All the results are recorded and statistically analyzed against the corresponding labels to evaluate the performance of the model. The training set would be used to train the model, the validation set for hyperparameter tuning and model selection (choosing the model that performs best on the validation set), and finally, the test set to validate the model.

Statistical analysis

X-tile 3.6.1 software [29] (Yale University, New Haven, CT, USA) was used to determine the optimal cut-off values. The optimal cut-off value is the best threshold used in fields like statistical analysis, medical diagnosis, and risk assessment to distinguish between different categories (such as "positive" and "negative"). This cut-off value is usually chosen at the point that maximizes the Youden Index. The maximum Youden Index point is calculated as the sum of sensitivity and specificity minus 1. Survival analysis was performed using the Kaplan-Meier method and Cox's proportional hazard model. We used Linear Regression. The Concordance Index (C-index), is a metric used to evaluate the predictive accuracy of a model. It is primarily employed to calculate the discrimination between the predicted values and the true values of the COX model in survival analysis. The C-index estimates the probability that the predicted outcomes are consistent with the actual observed outcomes, making it one of

Table 1 Characteristics in the training, test, and validation cohorts

	Training set($N=175$)	Test set($N=75$)	*P*
Age(years)			0.462
≤ 30	29	11	
≥ 70	31	13	
30–50	47	19	
50–70	68	32	
Sex			0.480
Female	97	35	
Male	78	40	
Tumor laterality			0.947
Left	86	37	
Right	89	38	
WHO grade			0.120
II	113	51	
III	62	24	
Tumor size, mean			0.357
	98.32	102.44	

the commonly used indicators in assessing the predictive accuracy of prognostic models for tumor patients. The Integrated Brier Score (IBS) is a metric utilized to assess the accuracy of probabilistic prediction models. Probabilistic prediction models are typically employed to forecast the probability of an outcome. IBS, one of the frequently used metrics for evaluating probabilistic prediction models, measures the discrepancy between the predicted outcomes and the actual outcomes. $P<0.05$ was considered statistically significant. All confidence intervals (CIs) were showed at the 95% confidence level.

Results

Of the 261 consecutive patients with a pathologic diagnosis of grade II or III meningiomas over a 2-year period from November 2021 until November 2023, 6 were excluded for poor MRI image quality (motion artifacts), 5 for lacking T1C and 250 patients were finally selected for the study. There were 164 patients with grade II and 86 patients with grade III. There were 118 males and 132 females in the entire dataset. The mean age of the patients was 52.72 years with a range of 15 to 79 years and the standard deviation was 14.34. We allocated 70% of the datasets to the training set (175 patients with 115 grade II and 60 grade III) and 30% of datasets to the independent test set (75 patients with 49 grade II and 26 grade III) (Table 1).

The interobserver agreements were good. There were 69,750 results generated from 279 feature values and 250 patients, which were too numerous to be displayed in full. In the article, we presented the results of WHO and gender using MinMax, Z-score and Mean normalization. After applying MinMax normalization, the results for WHO grade and gender were as follows: WHO grade II = 0, WHO grade III = 1; for gender, female = 0, and male = 1. After applying Z-score normalization, the results for WHO grade and gender were as follows: WHO grade II = -0.5883, WHO grade III = 1.69967; for gender, female = -0.8328, and male = 1.20077. After applying Mean normalization, the results for WHO grade and gender were as follows: WHO grade II = -0.2571, WHO grade III = 0.74286; for gender, female = -0.4095, and male = 1.59048.

The pipeline using MinMax_PCC_Cluster_19 of T2WI yielded the highest efficiency with an IBS of 0.189, 0.175, 0.185 and C-index of 0.783, 0.66, 0.649 in the train, test and validation sets, respectively (Fig. 1a). WHO grade, Mean and WavEnLL_s-2 were identified as the significant recurrence factors ($p=0.01$, 0.03, 0.03) (Table 2). $\chi2$ of WHO grade was 13.969 ($P=0.006$). The optimal cut-off value for Mean and WavEnLL_s-2 were 83.50 ($\chi2=10.247$, $P=0.034$) and 7984 ($\chi2=9.734$, $P=0.042$) (Fig. 2a-b).

The pipeline using Mean_PCC_Cluster_10 of T1C yielded the highest efficiency with an IBS of 0.170, 0.188, 0.208 and C-index of 0.709, 0.705, 0.602 in the train, test and validation sets (Fig. 1b). Age and Teta1 were identified as the significant recurrence factors ($p=0.01$, 0.03) (Supplementary Material 1). The optimal cut-off value for age and Teta1 were 66 ($\chi2=4.055$, $P=0.447$) and 0.90 ($\chi2=10.839$, $P=0.026$) (Fig. 2c).

The pipeline using MinMax_PCC_Cluster_13 of T2WI + T1C yielded the highest efficiency with an IBS of 0.152, 0.164, 0.191 and C-index of 0.701, 0.656, 0.593 in the train, test and validation sets, respectively (Fig. 1c). Age, gender, Perc.90%, Perc.99%, S(3, -3)DifVarnc, S(5, 5) Correlat, S(1, 0)SumEntrp, S(2, -2)InvDfMom and GrVariance were identified as the significant recurrence factors ($p<0.05$) (Supplementary Material 2). $\chi2$ of gender was 0.030 ($P=1.000$). The optimal cut-off value for age, Perc.90%, Perc.99%, S(3, -3)DifVarnc, S(5, 5)Correlat, S(1, 0)SumEntrp, S(2, -2)InvDfMom and GrVariance were 56 ($\chi2=9.723$, $P=0.042$), 190 ($\chi2=9.219$, $P=0.053$), 198 ($\chi2=9.713$, $P=0.042$), 7.70 ($\chi2=5.805$, $P=0.229$), 0.30 ($\chi2=5.629$, $P=0.248$), 1.10 ($\chi2=3.369$, $P=0.575$), 0.40 ($\chi2=7.574$, $P=0.107$) and 0.50 ($\chi2=10.764$, $P=0.026$) (Fig. 3).

Discussion

The necessity for new analytical methods beyond traditional statistical approaches, driven by big data, led to the emergence of the interdisciplinary field of knowledge discovery and data mining, which aims to uncover

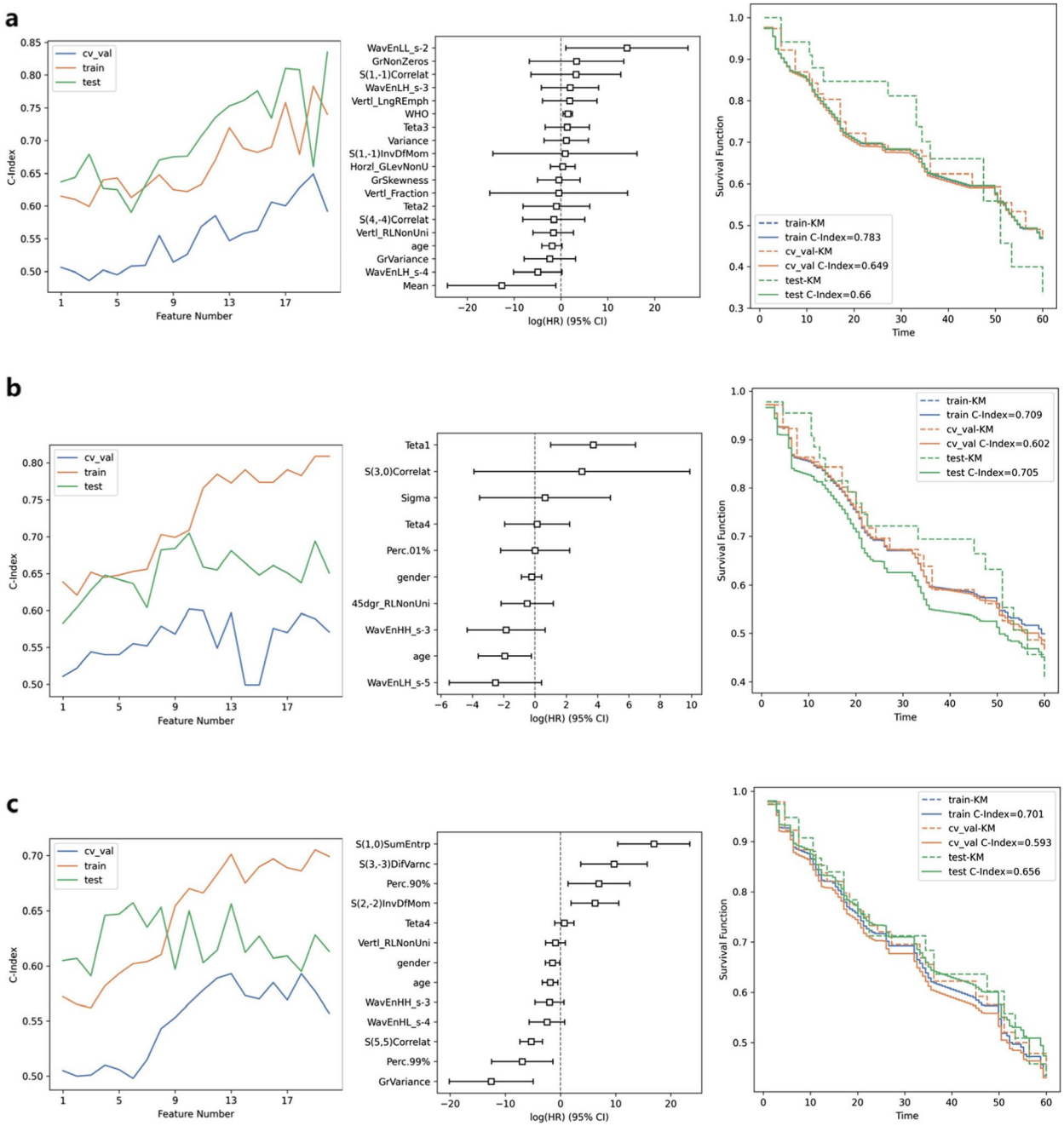

Fig. 1 (a) MinMax_PCC_Cluster_19 of T2WI; (b) Mean_PCC_Cluster_10 of T1C; (c) MinMax_PCC_Cluster_13 of T2WI+T1C; Feature number obtained(left panel); Feature Contribution (middle panel); C-index of the train and test sets(right panel)

new knowledge from data mines. In this study, we have attempted to explore the usability of KDD-based MRI radiomic features to assess relapse risk in patients with high-grade meningiomas. Statistical analysis of the radiomics was carried out to determine the most feasible features that involve WHO grade, age, Mean, Perc.99%, WavEnLL_s-2, Teta1 and GrVariance.

A comprehensive meta-analysis encompassing thirteen observational studies and 1243 patients revealed that the WHO grading of meningiomas stands as the most potent risk factor predictive of recurrence [30]. WHO grade II meningiomas, as well as a composite group encompassing both WHO grades II and III, exhibited a significantly elevated risk of recurrence compared to benign lesions.

Table 2 Comparison of radiomics features of MinMax_PCC_Cluster_19 of T2WI

Covariate	Coef	Exp (coef)	Se (coef)	Coef lower 95%	Coef upper 95%	Exp(coef) lower 95%	Exp(coef) upper 95%	Z	*P*	-log2(*p*)
Variance	1.10	3.01	2.42	-3.64	5.84	0.03	343.47	0.46	0.65	0.62
Vertl_Fraction	-0.51	0.60	7.51	-15.22	14.21	0.00	1.49E + 06	-0.07	0.95	0.08
S(1,-1)InvDfMom	0.86	2.37	7.85	-14.53	16.25	0.00	1.14E + 07	0.11	0.91	0.13
S(4,-4)Correlat	-1.53	0.22	3.38	-8.15	5.08	0.00	161.23	-0.45	0.65	0.62
Vertl_LngREmph	1.85	6.39	2.96	-3.95	7.66	0.02	2128.87	0.63	0.53	0.91
Mean	-12.67	0.00	5.91	-24.26	-1.09	0.00	0.34	-2.14	0.03	4.97
GrSkewness	-0.49	0.62	2.32	-5.04	4.07	0.01	58.36	-0.21	0.83	0.26
Teta2	-1.00	0.37	3.63	-8.10	6.11	0.00	450.89	-0.27	0.78	0.35
GrNonZeros	3.29	26.91	5.14	-6.79	13.37	0.00	6.41E + 05	0.64	0.52	0.94
WHO	1.42	4.16	0.52	0.41	2.43	1.51	11.42	2.76	0.01	7.45
GrVariance	-2.41	0.09	2.80	-7.89	3.08	0.00	21.69	-0.86	0.39	1.36
WavEnLH_s-3	1.92	6.82	3.12	-4.19	8.03	0.02	3058.6	0.62	0.54	0.89
Teta3	1.31	3.72	2.40	-3.39	6.02	0.03	410.63	0.55	0.58	0.78
Vertl_RLNonUni	-1.67	0.19	2.21	-5.99	2.66	0.00	14.25	-0.76	0.45	1.15
WavEnLH_s-4	-4.97	0.01	2.64	-10.14	0.19	0.00	1.21	-1.89	0.06	4.08
Horzl_GLevNonU	0.35	1.42	1.35	-2.30	3.00	0.10	20.17	0.26	0.79	0.33
S(1,-1)Correlat	3.17	23.76	4.90	-6.43	12.77	0.00	3.50E + 05	0.65	0.52	0.95
age	-1.94	0.14	1.09	-4.09	0.20	0.02	1.22	-1.78	0.08	3.73
WavEnLL_s-2	14.06	1.28E + 06	6.66	1.01	27.11	2.74	5.95E + 11	2.11	0.03	4.85

However, when comparing grade II and III lesions specifically, the odds of recurrence were found to be similar. While Han et al. [31] previously reported that the WHO grade did not achieve statistical significance in terms of recurrence, our findings contradict this, revealing that the recurrence rate does indeed increase with higher tumor grade. This observation aligns with those made in previous studies [32], indicating a clear correlation between tumor grade and the likelihood of recurrence. The majority of WHO grade II meningiomas underwent Simpson grade II and III resection procedures, with a minority undergoing grade I resection, resulting in a recurrence rate of 28.6%. In contrast, the majority of WHO grade III meningiomas were treated with Simpson grade II and III resections, and a few were subjected to grade IV resection, yielding a higher recurrence rate of 37.5%. It is generally acknowledged that the completeness of the original surgical removal plays a pivotal role in the prevention of postoperative recurrence of meningiomas [33]. However, certain types of meningiomas, particularly those that invade major venous sinuses, pose a challenge to complete resection, necessitating subtotal removal as a viable option [34]. Unfortunately, this approach is associated with a significantly higher rate of tumor recurrence [35], potentially stemming from the adoption of a less aggressive treatment strategy.

In the field of radiomics, data analysis incorporates the application of first-, second-, and sophisticated higher-level statistical metrics [36]. Firstly, when it comes to first-order statistics, they are characterized as the distribution of isolated voxel intensities without considering their spatial positioning or interactions. Commonly, they are histogram-derived metrics that characterize the statistical properties of pixel values contained within the defined ROIs, including the Mean and Perc.99%. The first-order ARM assumes that pixel intensity could be predicted as the weighted sum of four neighboring pixel intensities that are left, top, top-left and top-right adjacent [37]. Teta1 was found to be one of the most promising parameters. Subsequently, second-order statistics encapsulate the texture characteristics, precisely detailing the statistical dependencies and correlations among voxels exhibiting similar or varying contrast values, such as the GrVariance. Lastly, higher-order statistics apply filter grids to images for extracting patterns, both repetitive and non-repetitive, such as wavelets, which are indicative of texture frequency components gleaned from the energy measurements within various channels. In this study, Mean, Perc.99%, Teta1, GrVariance and WavEnLL_s-2 values were found to be the most promising parameters for assessing relapse risk in patients with HGMs. The characteristics of HGMs are losing normal

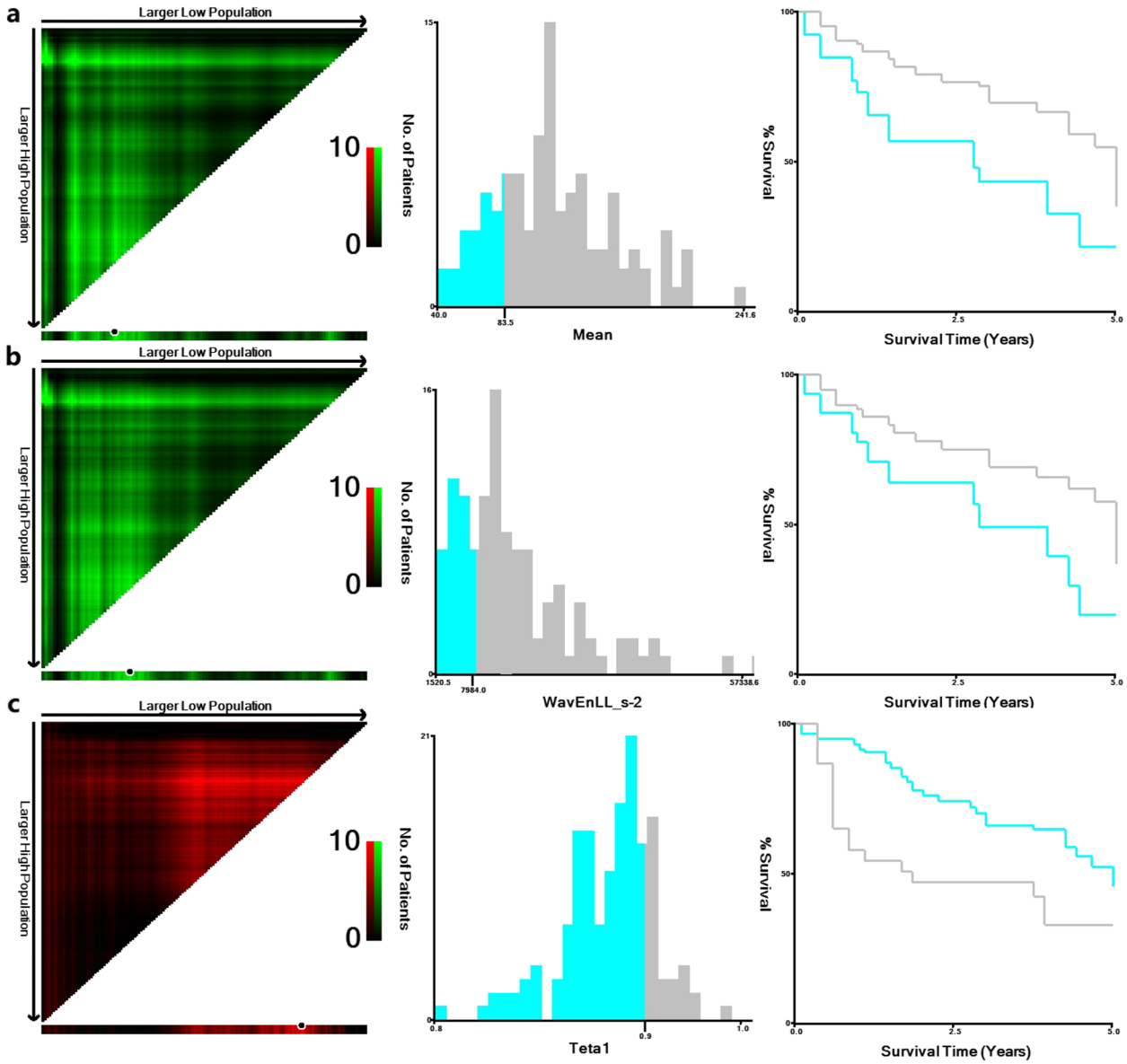

Fig. 2 Determination of the optimal cut-off values of Mean, WavEnLL_s-2 and Teta1 and survival analyses. X-tile plots of training sets are shown in the left panels, with plots of test sets shown in the smaller inset. The optimal cut-off values highlighted by the black circles in left panels are shown in histograms of the entire cohort (middle panels), and Kaplan-Meier plots are displayed in right panels. P values were determined by using the cut-off values defined in training sets and applying them to test sets

tissue or cell structure and focal necrosis, and these features lead to greater heterogeneity. Although the MRI signals of HGMs and LGMs are generally the same, the signals of HGMs are more variable [38].In the current study, the occurrence of tumors with flow voids was higher in grade III tumors than tumors with II grade. Most of the atypical meningiomas (WHO grade II) showed moderate enhancement, and anaplastic tumors (WHO grade III) were given priority when there was obvious and moderate heterogeneous enhancement [39]. HGMs are characterized by genomic instability [40, 41], which may be the basis of meningioma cell proliferation and tumor recurrence.

Our study has limitations. First, analyses should be performed in future studies after obtaining a larger sample size with automated or semi-automatic segmentation to determine the boundary. Second, as only T1C and T2WI maps were chosen, ADC and functional sequences will be expected to get a robust model.

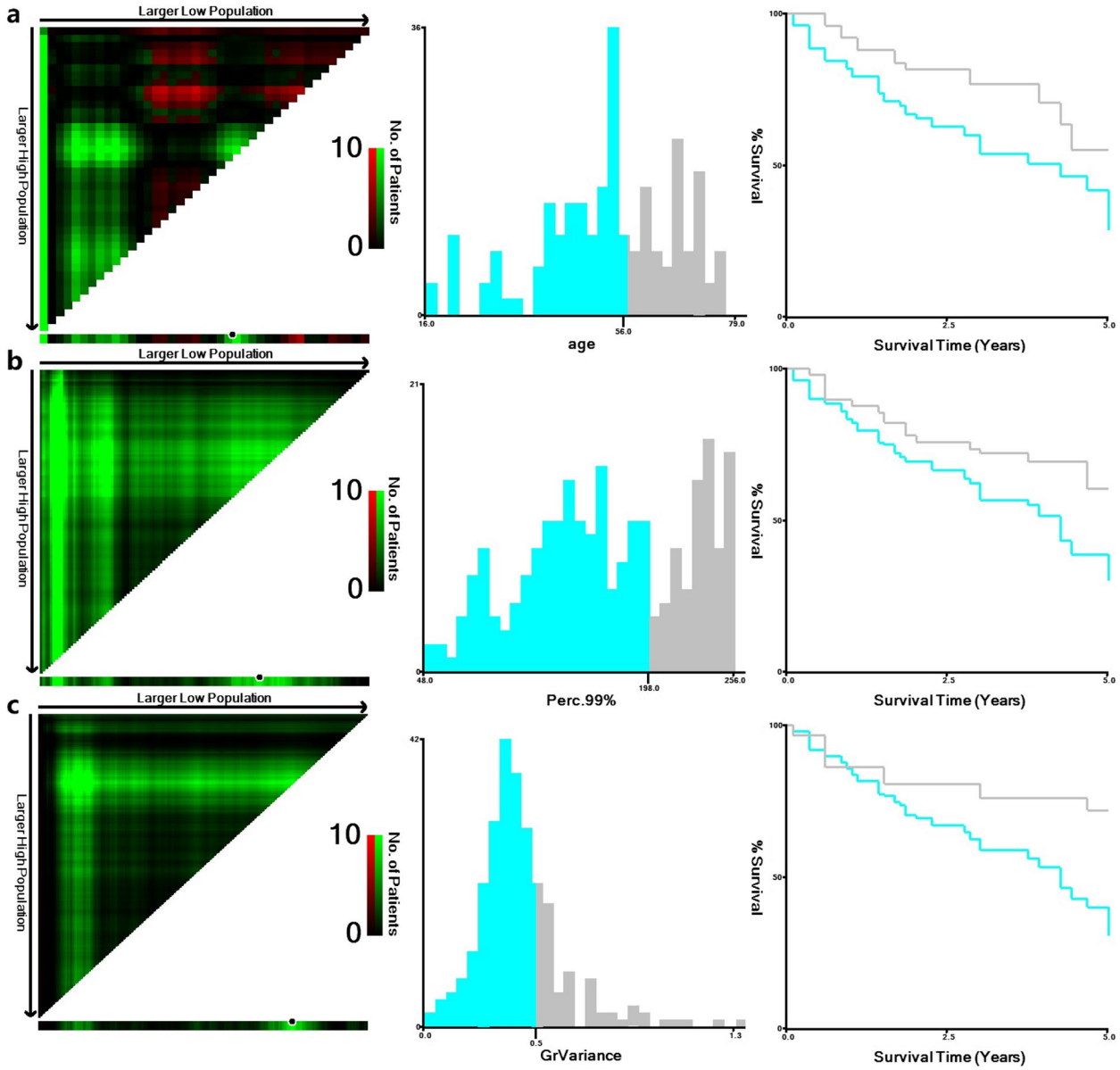

Fig. 3 Determination of the optimal cut-off values of age, Perc.99% and GrVariance and survival analyses

Conclusion

In this study, we investigated the feasibility of KDD-based radiomic models from T2WI and TIC maps values to slightly predict recurrence risk in HGMs. This prediction model has some potential to guide clinical prognosis prediction and decision-making for therapy in the future.

Abbreviations

KDD	Knowledge Discovery from Databases
T2WI	T2-weighted imaging
T1C	Contrast-enhanced T1-weighted imaging
HGMs	High-grade meningiomas
PCC	Pearson correlation coefficient
C-index	Concordance index
IBS	Integrated brier score
LGMs	Low-grade meningiomas
MRI	Magnetic resonance imaging
GLCM	Gray-level co-occurrence matrix
GLRLM	Gray-level run-length matrix
ARM	Auto-regressive model
WAV	Wavelets transform
AGS	Absolute gradient statistics

Supplementary Information

The online version contains supplementary material available at https://doi.org/10.1186/s12880-024-01483-2.

Supplementary Material 1.

Supplementary Material 2.

Acknowledgements
Thanks to all the peer reviewers and editors for their opinions and suggestions.

Authors' contributions
All authors contributed to the study conception and design. Material preparation, data collection and analysis were performed by Chen Chen, Lifang Hao, Bin Bai and Guijun Zhang. The first draft of the manuscript was written by Chen Chen and all authors commented on previous versions of the manuscript. All authors read and approved the final manuscript.

Funding
The research received no funding grant from any funding agency in the public, commercial, or not-for-profit sectors.

Data availability
The datasets used and/or analysed during the current study are available from the corresponding author on reasonable request.

Declarations

Ethics approval and consent to participate
All the experiment protocol for involving human data was in accordance with the guidelines of Declaration of Helsinki and the study was approved by the ethics review board of the Henan Provincial People's Hospital (2021 — 150). Written informed consent was obtained from every patient.

Consent for publication
Not applicable.

Competing interests
The authors declare no competing interests.

Author details
[1]Department of Radiology, Henan Provincial People's Hospital and Zhengzhou University People's Hospital, Henan Province No. 7 Weiwu, Zhengzhou City, China. [2]Department of Radiology, Liao Cheng The Third People's Hospital, Liaocheng, China. [3]Department of Neurosurgery, Tianjin Fifth Central Hospital, Tianjin, People's Republic of China. [4]Department of Neurosurgery, Shandong Provincial Hospital Affiliated to Shandong First Medical University, Jinan, China.

Received: 11 July 2024 Accepted: 29 October 2024
Published online: 09 January 2025

References

1. Ostrom QT, Patil N, Cioffi G, et al. CBTRUS statistical report: primary brain and other central nervous system tumors diagnosed in the United States in 2013–2017. Neuro Oncol. 2020;22(12 Suppl 2):v1-96. https://doi.org/10.1093/neuonc/noaa200.
2. Kshettry VR, Ostrom QT, Kruchko C, et al. Descriptive epidemiology of World Health Organization grades II and III intracranial meningiomas in the United States. Neuro Oncol. 2015;17(8):1166–73. https://doi.org/10.1093/neuonc/nov069.
3. Ostrom QT, Gittleman H, Liao P, et al. CBTRUS Statistical Report: primary brain and other central nervous system tumors diagnosed in the United States in 2010–2014. Neuro Oncol. 2017;19(suppl5):v1-88. https://doi.org/10.1093/neuonc/nox158.
4. Maggio I, Franceschi E, Tosoni A, et al. Meningioma: not always a benign tumor. A review of advances in the treatment of meningiomas. CNS Oncol. 2021;10(2):S72. https://doi.org/10.2217/cns-2021-0003.
5. Liu Z, Wang S, Dong D, et al. The applications of radiomics in precision diagnosis and treatment of oncology: opportunities and challenges. Theranostics. 2019;9(5):1303–22. https://doi.org/10.7150/thno.30309.
6. Villanueva-Meyer JE, Chang P, Lupo JM, et al. Machine learning in neurooncology imaging: from study request to diagnosis and treatment. AJR Am J Roentgenol. 2019;212(1):52–6. https://doi.org/10.2214/AJR.18.20328.
7. Senders JT, Zaki MM, Karhade AV, et al. An introduction and overview of machine learning in neurosurgical care. Acta Neurochir (Wien). 2018;160(1):29–38. https://doi.org/10.1007/s00701-017-3385-8.
8. Pattanaik BB, Anitha K, Rathore S, et al. Brain tumor magnetic resonance images classification based machine learning paradigms. Contemp Oncol (Pozn). 2022;26(4):268–74. https://doi.org/10.5114/wo.2023.124612.
9. Krahling H, Musigmann M, Akkurt BH, et al. A magnetic resonance imaging based radiomics model to predict mitosis cycles in intracranial meningioma. Sci Rep. 2023;13(1):969. https://doi.org/10.1038/s41598-023-28089-y.
10. Wang C, You L, Zhang X, et al. A radiomics-based study for differentiating parasellar cavernous hemangiomas from meningiomas. Sci Rep. 2022;12(1):15509. https://doi.org/10.1038/s41598-022-19770-9.
11. Musigmann M, Akkurt BH, Krahling H, et al. Assessing preoperative risk of STR in skull meningiomas using MR radiomics and machine learning. Sci Rep. 2022;12(1):14043. https://doi.org/10.1038/s41598-022-18458-4.
12. Zhao Y, Xu J, Chen B, et al. Efficient prediction of Ki-67 Proliferation Index in meningiomas on MRI: from traditional radiological findings to a machine learning approach. Cancers (Basel). 2022;14(15). https://doi.org/10.3390/cancers14153637.
13. Hsieh HP, Wu DY, Hung KC, et al. Machine learning for prediction of recurrence in Parasagittal and Parafalcine meningiomas: Combined Clinical and MRI texture Features[J]. J Pers Med. 2022;12(4). https://doi.org/10.3390/jpm12040522.
14. Bhattacharjee S, Prakash D, Kim CH, et al. Texture, morphology, and statistical analysis to differentiate primary brain tumors on two-dimensional magnetic resonance imaging scans using artificial intelligence techniques. Healthc Inf Res. 2022;28(1):46–57. https://doi.org/10.4258/hir.2022.28.1.46.
15. Yang L, Xu P, Zhang Y, et al. A deep learning radiomics model may help to improve the prediction performance of preoperative grading in meningioma. Neuroradiology. 2022;64(7):1373–82. https://doi.org/10.1007/s00234-022-02894-0.
16. Sun K, Zhang J, Liu Z, et al. A deep learning radiomics analysis for identifying sinus invasion in patients with meningioma before operation using tumor and peritumoral regions. Eur J Radiol. 2022;149: 110187. https://doi.org/10.1016/j.ejrad.2022.110187.
17. Khanna O, Fathi KA, Farrell CJ, et al. Machine learning using multiparametric magnetic resonance imaging radiomic feature analysis to predict Ki-67 in World Health Organization grade I Meningiomas. Neurosurgery. 2021;89(5):928–36. https://doi.org/10.1093/neuros/nyab307.
18. Ko CC, Zhang Y, Chen JH, et al. Pre-operative MRI radiomics for the prediction of progression and recurrence in Meningiomas. Front Neurol. 2021;12: 636235. https://doi.org/10.3389/fneur.2021.636235.
19. Kalasauskas D, Kronfeld A, Renovanz M, et al. Identification of high-risk atypical meningiomas according to Semantic and Radiomic Features[J]. Cancers (Basel). 2020;12(10). https://doi.org/10.3390/cancers12102942.
20. Szczypiński PM, Klepaczko A. Chapter 11 - MaZda – A framework for biomedical image texture analysis and data exploration[M]. Biomed Texture Anal. 2017:315–4. https://doi.org/10.1016/B978-0-12-812133-7.00011-9.
21. Strzelecki M, Szczypinski P, Materka A, Klepaczko A. A software tool for automatic classification and segmentation of 2D/3D medical images. Nuclear Instrum Methods Phys Res A. 2013;702:137–40.
22. Szczypinski PM, Strzelecki M, Materka A, Klepaczko A. MaZda - the software package for textural analysis of biomedical images. Adv Intell Soft Comput. 2009;65:73–84.
23. Szczypinski P, Strzelecki M, Materka A, Klepaczko A. MaZda - A software package for image texture analysis. Comput Methods Programs Biomed. 2009;94(1):66–76.
24. Collewet G, Strzelecki M, Mariette F. Influence of MRI acquisition protocols and image intensity normalization methods on texture classification. Magn Reson Imaging. 2004;22(1):81–91. https://doi.org/10.1016/j.mri.2003.09.001.
25. Castellano G, Bonilha L, Li LM, et al. Texture analysis of medical images. Clin Radiol. 2004;59(12):1061–9. https://doi.org/10.1016/j.crad.2004.07.008.
26. S RMHK. Textural features for image classification. IEEE Trans Syst Man Cybernetics SMC. 1973;3(6):610–21. https://doi.org/10.1109/TSMC.1973.4309314.

27. Galloway MM. Texture analysis using gray level run lengths. Comput Graphics Image Process. 1975;4(2):172–9. https://doi.org/10.1016/S0146-664X(75)80008-6.
28. Orphanidou-Vlachou E, Vlachos N, Davies NP, et al. Texture analysis of T1 - and T2 -weighted MR images and use of probabilistic neural network to discriminate posterior fossa tumours in children. NMR Biomed. 2014;27(6):632–9. https://doi.org/10.1002/nbm.3099.
29. Camp RL, Dolled-Filhart M, Rimm DL. X-tile: a new bio-informatics tool for biomarker assessment and outcome-based cut-point optimization. Clin Cancer Res. 2004;10(21):7252–9. https://doi.org/10.1158/1078-0432.CCR-04-0713.
30. Balik V, Kourilova P, Sulla I, et al. Recurrence of surgically treated parasagittal meningiomas: a meta-analysis of risk factors. Acta Neurochir (Wien). 2020;162(9):2165–76. https://doi.org/10.1007/s00701-020-04336-3.
31. Han MS, Kim YJ, Moon KS, et al. Lessons from surgical outcome for intracranial meningioma involving major venous sinus. Med (Baltim). 2016;95(35): e4705. https://doi.org/10.1097/MD.0000000000004705.
32. Yu J, Chen FF, Zhang HW, et al. Comparative analysis of the MRI characteristics of meningiomas according to the 2016 WHO pathological Classification. Technol Cancer Res Treat. 2020;19:1079250935. https://doi.org/10.1177/1533033820983287.
33. Black PM. Meningiomas. Neurosurgery. 1993;32(4):643–57. https://doi.org/10.1227/00006123-199304000-00023.
34. Sindou M. Meningiomas invading the sagittal or transverse sinuses, resection with venous reconstruction[J]. J Clin Neurosci. 2001;8(Suppl 1):8–11. https://doi.org/10.1054/jocn.2001.0868.
35. Murata J, Sawamura Y, Saito H, et al. Resection of a recurrent parasagittal meningioma with cortical vein anastomosis: technical note. Surg Neurol. 1997;48(6):592–5. https://doi.org/10.1016/s0090-3019(97)00303-0.
36. Gillies RJ, Kinahan PE, Hricak H. Radiomics: images are more than pictures, they are Data. Radiology. 2016;278(2):563–77. https://doi.org/10.1148/radiol.2015151169.
37. Szczypinski PM, Strzelecki M, Materka A, et al. MaZda–a software package for image texture analysis. Comput Methods Programs Biomed. 2009;94(1):66–76. https://doi.org/10.1016/j.cmpb.2008.08.005.
38. Magill ST, Vasudevan HN, Seo K, et al. Multiplatform genomic profiling and magnetic resonance imaging identify mechanisms underlying intratumor heterogeneity in meningioma. Nat Commun. 2020;11(1):4803. https://doi.org/10.1038/s41467-020-18582-7.
39. Masalha W, Heiland DH, Delev D, et al. Survival and prognostic predictors of anaplastic Meningiomas. World Neurosurg. 2019;131:e321-8. https://doi.org/10.1016/j.wneu.2019.07.148.
40. Bi WL, Greenwald NF, Abedalthagafi M, et al. Genomic landscape of high-grade meningiomas. NPJ Genom Med. 2017;2:15. https://doi.org/10.1038/s41525-017-0014-7.
41. Williams EA, Santagata S, Wakimoto H, et al. Distinct genomic subclasses of high-grade/progressive meningiomas: NF2-associated, NF2-exclusive, and NF2-agnostic[J]. Acta Neuropathol Commun. 2020;8(1):171. https://doi.org/10.1186/s40478-020-01040-2.

Publisher's Note